Proceedings of the 25th International Conference on
Port and Ocean Engineering under Arctic Conditions
June 9-13, 2019, Delft, The Netherlands

On the influence of the hydraulic characteristics of the rig during full-scale compression and indentation tests on sea ice

Aleksey Marchenko[1], Evgeny Karulin[2], Alexander Sakharov[3], Peter Chistyakov[3]
[1] The University Centre in Svalbard, Longyearbyen, Norway
[2] State Marine Technical University, St.-Petersburg, Russia
[3] Lomonosov Moscow State University, Moscow, Russia

ABSTRACT

A model of the hydraulic rig was constructed and validated using the data of calibration tests performed to estimate internal elasticity and viscosity of the rig. A steel frame to constrain an extension of the rig was designed and constructed to estimate an effective elastic modulus of the loading system. The effective rig viscosity was estimated by measuring the accelerations during a test by suddenly releasing of the load applied to the rig by failure a strap loop, that was fixed around the rig. Equations describing the motion of the plunger and indentation plate were derived using the mass balance of the oil and the momentum balance of the rig. Numerical simulations were performed to investigate the dependence between the measured displacements and loads and the actual displacements of indentation plate relative to the ice and the loads applied to the indentation plate. It has been shown that these to be very close to each other in the full-scale tests on brittle failure of a short cantilever beams by compression.

KEY WORDS: hydraulic rig, full-scale tests, sea ice.

INTRODUCTION

Conducting of mechanical strength tests with big samples always relates to the difficulties of mounting a big sample in a rig whose sizes are limited by logistic and other constrains. Local deformations of the mounts and material may influence the recorded data on displacements, which include the deformations of sample and rig both. Stiffness of the testing rig may also influence the interaction between the rig and sample, which is not registered but can be important for material behavior under high loads. Such situation has been observed during tests having stick-sleep interaction between ice and steel (Sukhorukov and Marchenko, 2014). In an experiment, steel rods with manufactured surface roughness were pushed through the holes in ice. The load was applied by compression rig Knekkis by a plunger powered by electric engine. Tests with constant load and constant rates of displacement were performed. During the tests, the steel rods experienced high accelerations during certain stages of their stick-slip motion, and the ends of the rods lost contact periodically from the plunger. Characteristics of the rig stiffness were introduced in a mathematical model to describe these observations.

In the present paper, we consider the interaction of a hydraulic rig designed to conduct full-scale-indentation tests on a floating ice sheet (Karulin et al., 2014). Hydraulically operated indentation rigs have earlier been designed and used in similar indentation tests (Croasdale, 1974,1977; Sodhi et al., 1998), but their interaction with ice has not been analyzed. In the first two sections of this paper, we describe the construction of the hydraulic rig and formulate a mathematical model to describe the action of the rig. In the third section, we describe the calibration procedures to obtain elastic and viscous characteristics of the rig from the calibration data. We discuss results of numerical simulations in the fourth section, and the main results of the study are formulated in the Conclusions.

CONSTRUCTION OF THE HYDRAULIC RIG

The equipment for the full-scale-ice-strength tests was designed at UNIS under the support of SAMCoT project in 2011. It comprises hydraulic rig mounted on a steel frame by tackles, two-stage hydraulic pump, three-phase-400-Volt generator, and field computer. The indenter rig consists of two hydraulic cylinders connected by four hinges to semi-cylindrical, or flat, indenters (Fig. 1). The upper and the lower hydraulic cylinders, shown in the right panel of Fig. 1, are named as A and B cylinders, respectively. To measure sea ice strength, the rig applies a load in the horizontal direction across the entire thickness of sea ice. Small indenter of spherical shape can be attached to the flat indenter (shown in the right panel of Fig. 1) to perform tests similar to those by a borehole-jack tests. The rig and the field computer were constructed by Maskin K Lund AS (http://www.mkl.no/) in 2011. Steel frame and indenters were manufactured in Henningsen workshop (https://www.htg.svalbard.no/).

The rig is suspended from an A-shaped steel frame to lower, or to rise, the indenters and the hydraulic cylinders into a previously cut hole in an ice sheet. The rig, frame, electrical pump, field computer and generator are placed on three sledges and can easily be transported by snow scooters to different places to conduct field tests. During each test the recorded data include the load, the stroke, and the oil pressure in each cylinder. The data are sampled at a rate of 100 Hz and recorded on a hard disk of the field computer and also on a data logger CR6. The backup of data recording and storage helps to avoid any loss of data during malfunction of one the recording system.

Each of the hydraulic cylinders (Enerpac) is equipped with a displacement sensor and a load cell. The stroke of the hydraulic cylinder is 37 cm, the load capacity of 300 kN, plunger diameter is 5 cm, and the effective area for the plunger pushing is 44.2 cm^2. Figure 2 shows a sketch demonstrating the construction and action of the hydraulic cylinder. An Arctic oil is pumped into, and from, each cylinder by two hoses. Figure 3 shows the characteristic of the electric, two-stage pump (Enerpac ZE5) in terms of oil flow – pressure chart. Two-stage pumps have an increased output flow at low pressure to allow fast movement towards the load to obtain, for reduced cycle times and increased productivity. It means that increased output flow is realized when the load on cylinder is smaller than 20% of the maximal load 300 kN, i.e. when the load per cylinder is below 60 kN. The discretization of converting analog signal to digital signal is 5 psi for the pressure signal, 0.22 mm for the stroke signal and 295 N for the load signal. The accuracy of the sensors is about 0.1% from the full range of measurements.

Figure 1. Hydraulic rig to conduct full-scale tests to measure ice strength. Left panel shows the indenter packed on sledges. Right panel shows an indenter mounted on an A-shaped frame with sledges.

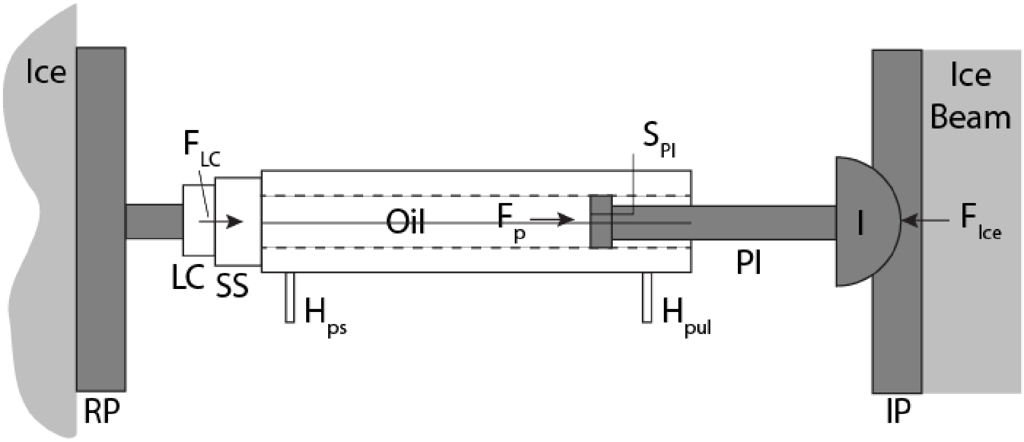

Figure 2. Sketch of the hydraulic rig, in which the abbreviated names decsrib the following: LC - load cell, SS - stroke sensor, Pl - plunger, I – semi-cylindrical indenter, IP – indentation plate, RP – root plate, S_{PL} – surface area of plunger.

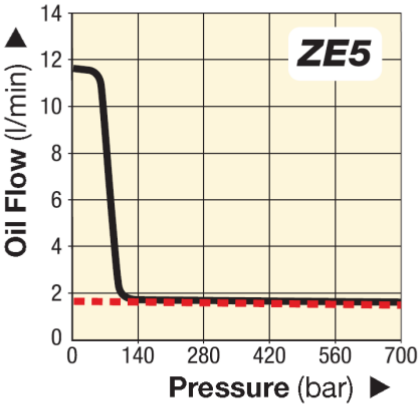

Figure 3. Oil flow – pressure chart for the electric pump Enerpac ZE5.

There is main valve to open and lock the oil flow from the hydraulic pump into the hydraulic cylinders. The valve can be fixed in three positions related to the locking, pumping and sucking of the oil from the cylinders into the tank. The hydraulic pump is equipped with a valve changing the rotor speed of the electrical engine in the pump. In addition, each of the two hoses Hps (Fig. 2) is equipped with a valve changing the oil flux into the cylinders. These valves are used to change indentation rate of the rig and to keep indentation plate in the vertical position. The valves are operated manually.

The characteristics of hydraulic cylinder, hydraulic pump and hydraulic oil are given in the following:

$$M_{HC} = 60 \text{ kg}, M_{Pl} = 10 \text{ kg}, S_{Pl} = 44.2 \text{ cm}^2, \tag{1}$$

$$L_{max} = 37 \text{ cm}, F_{max} = 300 \text{ kN}, q_{min} = 1.64 \text{ l/min},$$

$$\rho_{oil} = 900 \text{ kg/m3}, k_{oil} = 2 \cdot 10^9 \text{ Pa},$$

where M_{HC} is the mass of the hydraulic cylinder, M_{Pl} is the mass of the plunger PL with hinge joint, S_{Pl} is the pushing area of the plunger (Fig. 2), L_{max} is the maximal stroke, and F_{max} is the maximal load, q_{min} is the minimal output flow rate of the hydraulic pump. The flat indenter consists of the semi-circular indenter I and indentation plate IP (Fig. 2). The estimated mass of the flat indenter is $M_{FI} = 200$ kg.

MATHEMATICAL MODEL OF THE HYDRAULIC RIG

Further, we consider a mathematical model to describe the dynamics of one hydraulic cylinder, assuming that each of the hydraulic cylinders in the rig are equally loaded. It is also assumed that the root plate RP is fixed, and a part of the cylinder comprising the load cell LC, the stroke sensor SS and hinge have some effective elasticity (Fig. 2). Further, we call this part as LC for simplification of notations. Momentum balance of the hydraulic cylinder without the plunger and momentum balance of the plunger with flat indenter are written in the form

$$(M_{HC} - M_{Pl})\frac{dv_{HC}}{dt} = F_{LC} - F_p - F_f, \tag{2}$$

$$(M_{Pl} + M_{FI}/2)\frac{dv_{Pl}}{dt} = F_p + F_f + F_{Ice}, \tag{3}$$

where M_{HC} is the mass of the hydraulic cylinder, M_{Pl} is the mass of the plunger, M_{FI} is the mass of the flat indentation plate with semi-circular indenter, v_{HC} and v_{Pl} are, respectively, the velocities of the hydraulic cylinder and indentation plate, F_p is the pressure force applied to the piston by oil, F_f is the friction force acting between the cylinder and the plunger, F_{LC} is elastic force due to the reaction of LC on compression, F_{Ice} is the force applied to the indentation plate by the ice beam, and t is the time. Positive velocities are directed to the ice beam in Fig. 2.

Mass balance of the oil is written as follows

$$\frac{d(\rho_{oil}V_{oil})}{dt} = \kappa q, \tag{4}$$

where ρ_{oil} is the oil density, V_{oil} is the oil volume inside the cylinder, q in the influx of the oil through the hose Hps, and κ is a time-dependent coefficient depending on the rotor speed and position of the middle valve (Fig. 2).

Kinematic condition at the piston edge located inside the cylinder is

$$\frac{dV_{oil}}{dt} = S_{Pl} v_{SS} \,, \tag{5}$$

where $v_{SS} = v_{Pl} - v_{HC}$ is the plunger velocity relative to the hydraulic cylinder. The plunger displacement is determined by the formula

$$x_{SS} = x_{Pl}\text{-}x_{HC}. \tag{6}$$

Absolute displacements x_{HC} and x_{Pl} of the hydraulic cylinder and the plunger are introduced by the formulas

$$\frac{dx_{HC}}{dt} = v_{HC}, \frac{dx_{Pl}}{dt} = v_{Pl}. \tag{7}$$

Forces F_p, F_f, and F_{LC} are specified by the following expressions

$$F_p = S_{Pl} p_{oil},\ F_f = -\mu v_{SS}, F_{LC} = -k_{LC} x_{HC}, \tag{8}$$

where p_{oil} is the oil pressure above the atmospheric pressure, μ is the coefficient of friction, and k_{LC} is the effective elastic modulus of LC.

The rate of change of oil pressure is specified by the equation given below

$$\frac{dp_{oil}}{dt} = \frac{k_{oil}}{\rho_{oil}} \frac{d\rho_{oil}}{dt}, \tag{9}$$

where k_{oil} is the compressibility, or the bulk modulus, of oil.

Equations (2) – (9) are reduced to the following equations

$$(M_{HC} - M_{Pl}) \frac{d^2 x_{HC}}{dt^2} = \mu v_{SS} - S_{Pl} p_{oil} - k_{LC} x_{HC}, \tag{10}$$

$$(M_{Pl} + M_{FI}/2) \frac{d^2 x_{Pl}}{dt^2} = S_{Pl} p_{oil} - \mu v_{SS}, \tag{11}$$

$$\frac{dp_{oil}}{dt} = -\frac{k_{oil}}{L_0} v_{SS}, \tag{12}$$

$$\frac{dx_{Pl}}{dt} - \frac{dx_{HC}}{dt} = v_{SS}, \tag{13}$$

when $q = 0$, $F_{Ice} = 0$, and $L_0 = V_{oil,0} S_{Pl}^{-1}$, where $V_{oil,0}$ is a constant characterizing amount of oil in the cylinder. The eigenvalues of equations (10)-(13) are the roots of the characteristic equation written in the dimensionless variables as follows:

$$(y^2 - 1)(a_1 y^2 - a_2) - y^2 = i\varepsilon y (y^2 (1 + a_1) - a_2), \tag{14}$$

where

$$y = \frac{\omega}{\omega_0},\ \omega_0^2 = \frac{k_{oil} S_{Pl}}{L_0 (M_{Pl} + M_{FI}/2)},\ a_1 = \frac{M_{HC} - M_{Pl}}{M_{Pl} + M_{FI}/2}, a_2 = \frac{k_{LC} L_0}{k_{oil} S_{Pl}},\ \varepsilon = \frac{\mu}{\omega_0 (M_{Pl} + M_{FI}/2)}.$$

Frequency $\omega_0 \approx 630$ rad/s is estimated with numerical values of physical constants specified by formulas (1) and $L_0 = 20$ cm. Equation (14) has two positive roots and two negative roots, and their absolute values are $y_1 \approx 0.73$ and $y_2 \approx 2.38$ when $\varepsilon = 0$. The roots correspond to oscillations with the dimensional periods of $T_1 \approx 0.013$ s and $T_2 \approx 0.004$ s. The existence two different absolute values of the roots of characteristic equation (14) for $\varepsilon = 0$ is explained by the construction of the hydraulic cylinder including two elastic elements associated with the spring in the load cell and with the compressibility of oil inside the hydraulic cylinder.

Figure 4 shows the locations of roots on a complex plane, calculated with the values of ε changing from 0 to 2.15. Blue circles show the roots with absolute values of y_1 and y_2 for $\varepsilon = 0$. The roots displace on the imaginary semi-plane $(Re[y], Im[y])$ with $Im[y] > 0$ when ε increases. Real parts of two roots become equal to 0 when $\varepsilon \approx 2$ or greater. Imaginary parts of these roots tend to 0 and ∞ when $\varepsilon \to \infty$. The other two roots tend to be real values of opposite signs when $\varepsilon \to \infty$. Their absolute value tends to be $a_2/(1 + a_1) \approx 0.93$. Green and brown points mark the roots calculated with nonzero values of the viscosity obtained in calibration tests and described in the next section.

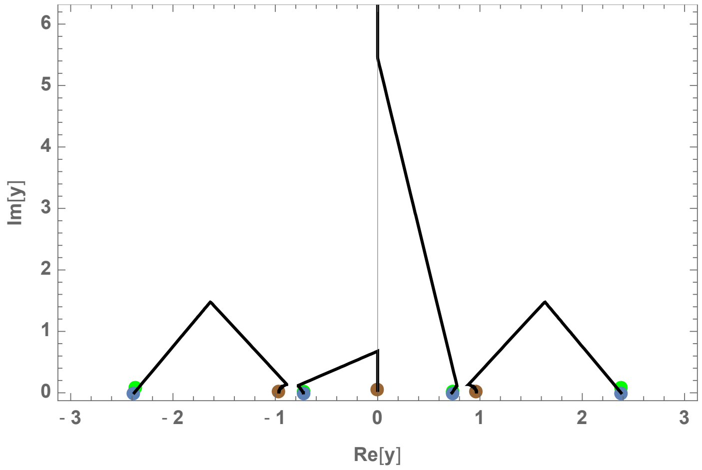

Figure 4. Lines show the location of the roots of equation (14) on a complex plane when ε increases from 0 to 2.15. Blue circles show the roots calculated for $\varepsilon = 0$. Green and brown points mark the roots calculated with nonzero values of the viscosity obtained in calibration tests.

CALIBRATION EXPERIMENTS

The rig with flat indentation plates was placed inside a frame welded from channel beams made of steel with h =6 mm in thickness (Fig. 5). The length of the frame in the parallel direction to the hydraulic cylinders was L_f =2.1 m. The beam width and height were b =13 cm and w =6 cm respectively. Each of the hydraulic cylinders was allowed to apply maximal load to the frame. The stroke sensor registered the displacement $x_{SS} = x_{Pl}$-x_{HC} when the load was applied to the frame by the hydraulic cylinders. The plunger displacement x_{Pl} is calculated from the formula

$$\frac{F_{LC}}{S_B} = 2E\frac{x_{Pl}}{L_f}, \quad S_B = (b + 2w)h, \qquad (15)$$

where S_B is the area of transverse cross-section of the beam, F_{LC} is the load measured by the load cell, and E is the elasticYoung’s modulus of steel.

The displacement x_{HC} of the hydraulic cylinder is calculated from the third formula (8). From (15) it follows

$$k_{LC} = \frac{2ES_B F_{LC}}{2ES_B x_{SS} - L_f F_{LC}}\,. \tag{16}$$

Figure 6 shows the results of three calibration tests by blue lines. The dependence of the force registered by the load cell F_{LC} from the displacement registered by the stroke sensor is close to the linear dependence shown in Fig. 6 by black line when $x_{SS} > 1$ mm. Using 1 mm as offset value for the displacement we find that the loads cells measured load 250 kN when the stroke sensors registered displacements of 5 mm. Substituting $F_{LC} = 250$ kN, $x_{SS} = 5$ mm and $E = 200$ GPa in formula (16) we find $k_{LC} = 0.6 \cdot 10^8$N/m.

The second set of experiments was performed to determine the friction coefficient μ between the plunger and hydraulic cylinder. The hydraulic rig was hung on a steel frames and strapped by a strap loop equipped with quick release hook (Fig. 7). The hook was released after the load in the top cylinder had reached 6 kN. The accelerations were recorded by an accelerometer (Dytran 4400A1 vibration recorder) (https://www.dytran.com/Model-4400A-VibraCorder-P3060/), which was mounted on the top of the semi-cylindrical indenter connected to the flat indentation plate. The sampling frequency was set to 1.6 kHz. The range of measurements of the Dytran was ±200 g and it recorded three components of acceleration in the Cartesian reference frame associated with the recorder.

Figure 5. Steel frame for the calibration of the indentation rig. The rig is inside the frame.

Figure 8 shows time-history plots of two records of the acceleration along the z – axis by blue and yellow lines. The direction of the z – axis is pointed out in Fig. 7. The first positive peak HR corresponds to the load increase during the quick release hook. Then blue line shows three oscillations with a period of about 10 ms. Total durations of the impulses are of about 40 ms on the both graphs. The period 10 ms corresponds to the frequency ω_0 given after formula (14). The friction coefficient is estimated with the formula

$$\mu \approx \frac{(M_{Pl} + M_{Fl}/2)\omega_0}{6\pi} = 3.7 \cdot 10^3 \text{ N·s/m}. \tag{17}$$

Green points in Fig. 4 show the locations of the roots of equation (14) when the friction coefficient is determined by formula (17). They are very close to the blue points showing the locations of the root when $\mu = 0$.

Estimation of the friction coefficient was also performed using the experiment when the hydraulic pump was working but the indentation plates were not loaded, i.e. the ice force equals to zero $F_{Ice} = 0$ in equations (2) and (3). Records of the strokes and oil pressure in the hydraulic cylinders A and B are shown in Fig. 9 versus the time. Signal fluctuations are explained by the discretization of converting analog signal to digital signal. The friction coefficients calculated from the balance $F_p + F_f = 0$ for each cylinder equal

$$\mu_A = 1.35 \cdot 10^6 \text{ N·s/m}, \; \mu_B = 4.46 \cdot 10^6 \text{ N·s/m}. \tag{18}$$

One can see that their values are greater on three orders than the value specified by formula (17). The roots of equation (14) calculated with the values of the friction coefficients specified by formulas (18) are shown by brown dots in Fig. 4. The values of two roots are close to $y = 1$ for $\mu = \mu_A$ and $\mu = \mu_B$. The third and the fourth roots are pure imaginary. The third root is close to 0, and the absolute value of the fourth root is greater than 50. Therefore, the fourth root is not shown in Fig. 4. Imaginary parts of the roots close to 1 are 0.016 by $\mu = \mu_A$, and 0.005 by $\mu = \mu_B$. It corresponds to e-folding times (the time interval in which an exponentially decaying quantity decreases by a factor of e) of about 0.1 s and 0.3 s. Such oscillations were not registered in the experiments on viscous damping of oscillations of the hydraulic cylinders (Fig. 7). Therefore, the friction coefficient depends on the frequency.

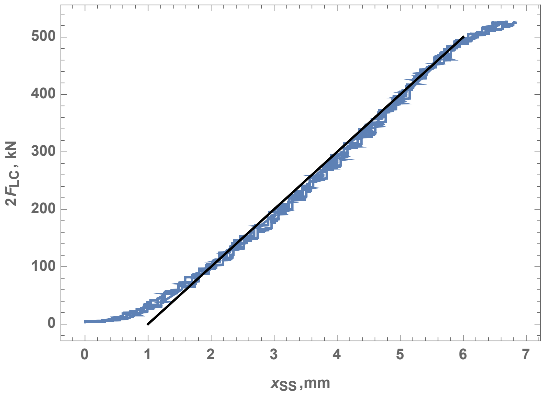

Figure 6. Force-displacement charts recorded in three calibration tests are shown by blue lines. Black line shows their linear extrapolation.

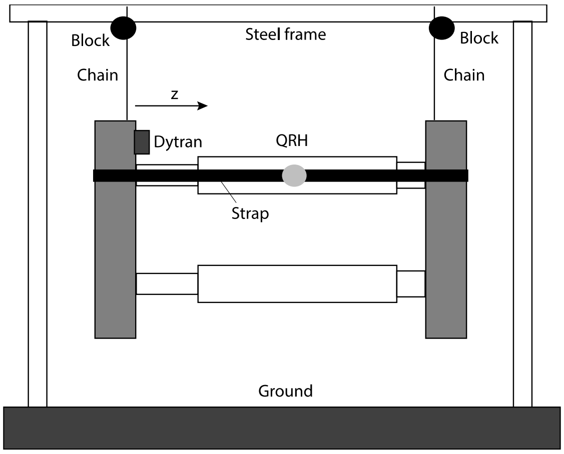

Figure 7. Sketch of the calibration test on viscous damping of oscillations of the hydraulic cylinders. QRH is quick release hook. The mounting location of the accelerometer Dytran is pointed out.

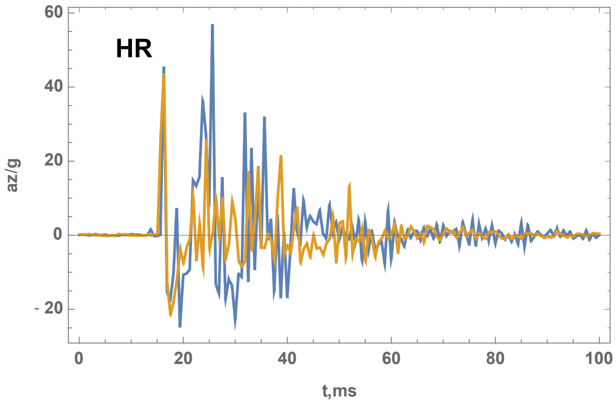

Figure 8. Time-history plot of accelerations of the semi-circular as recorded during two tests on viscous damping.

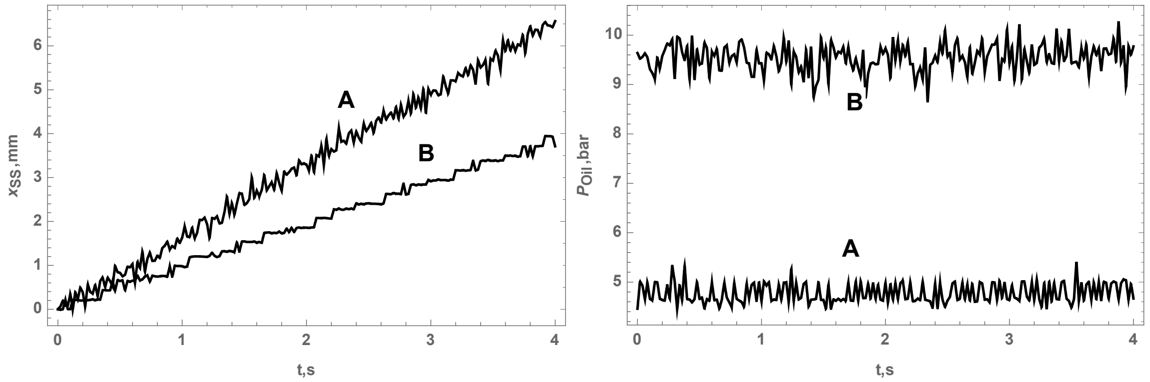

Figure 9. Records of the strokes (left panel) and oil pressures in the cylinders A and B (right panel) in the experiment without a load on the indentation plate.

NUMERICAL SIMULATIONS

Equations (2)-(9) can be reduced to the system of three equations relative to the variable $x_{Pl}(t)$, $x_{SS}(t)$, and p_{oil}

$$(M_{HC}-M_{Pl})\frac{d^2(x_{Pl}-x_{SS})}{dt^2} = -k_{LC}(x_{HC}-x_{SS}) - S_{Pl}p_{oil} + \mu\frac{dx_{PSS}}{dt}, \tag{19}$$

$$(M_{Pl}+M_{FI}/2)\frac{d^2x_{Pl}}{dt^2} = S_{Pl}p_{oil} + \mu\frac{dx_{PSS}}{dt} + F_{Ice}, \tag{20}$$

$$\frac{dp_{oil}}{dt} = \frac{\rho_{oil}}{S_{Pl}x_{SS}}\left(\kappa q - S_{Pl}\frac{dx_{PSS}}{dt}\right). \tag{21}$$

The flux q is specified by the formula according to Fig. 3

$$q = q_0(6.645 - 4.965\ \tanh[0.05(p_{oil}-p_{max})]), \tag{22}$$

where $q_0 = 1$ l/min, and $p_{max} = 700$ bar.

Equations (19)-(22) were investigated numerically using Wolfram Mathematica 11.2 Software. The ice force was taken from the records of the load cells during the full-scale test on the compression of short cantilever beams (Marchenko et al., 2018) performed on March 2018 in the Van Mijen Fjord, Spitsbergen. Left panel in Fig. 10 shows the loads recorded by the load cells in the hydraulic cylinders A and B. Most important part of the test is extended from $t = 25$ s to $t = 50$ s. During this time the indentation plate had full contact with the end of the cantilever beam and compressed it in the axial direction until the beam failure took place.

The recorded loads were substituted in equations (20) to model the ice forces F_{Ice} on the indentation plates near the cylinders A and B. The coefficients κ was taken equal to 0.2 and 0.12 for the cylinders A and B respectively. Numerical simulations were performed with the initial conditions

$$x_{Pl} = x_{SS} = 0.2 \text{ mm}, x'_{Pl} = x'_{SS} = 0, p_{oil} = 0, t = 0. \qquad (23)$$

Right panel in Fig. 10 shows the simulated and the recorded pressure in the oil. Left panel in Fig. 11 shows the simulated and the recorded displacements of the plungers in the cylinders A and B. Since the ice force on the cylinder B was smaller than the force on the cylinder A (Left panel in Fig. 10) the speed of the cylinder B was higher than that in the cylinder A in the beginning of the test. Therefore, the middle valve on the hose Hps connecting the pump and the cylinder was placed in the position corresponding zero oil flux when $t = 25$ s, and then open again. The simulations were performed with constant value of the coefficient $\kappa = 0.12$. It influenced divergence of the recorded and the simulated displacements in the cylinder B shown in left panel of Fig. 11.

Right panel in Fig. 11 shows very small deviation of the simulated displacements x_{Pl} from the simulated displacements x_{SS}. It demonstrates that displacements recorded by stroke sensors is very close to the actual displacements of the indentation plate. Numerical estimates also showed that the deviations of the loads shown in left panel in Fig. 10, which were used to model the force F_{Ice} in the numerical simulations, from the simulated loads F_{LC} is smaller than 0.003%. It demonstrates that the forces measured by the load cells are very close to the actual forces applied by ice to the indentation plate.

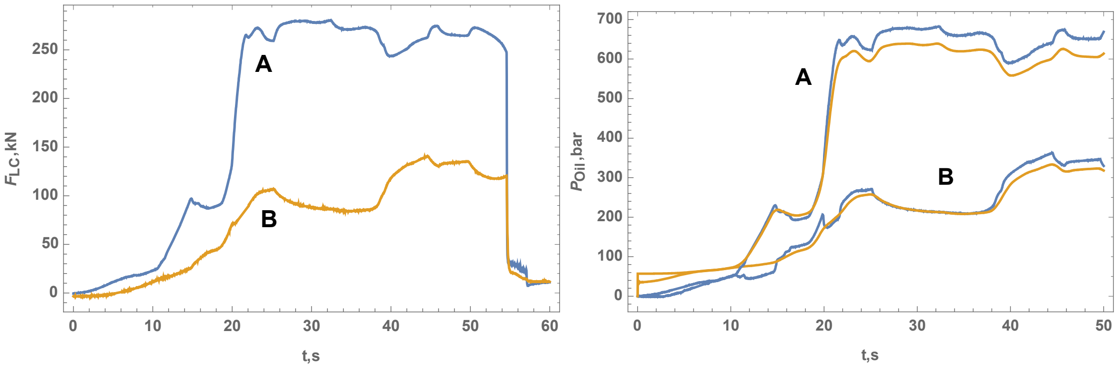

Figure 10. Left panel: Records of the loads measured by the load cells in the cylinders A and B during the full-scale tests. Right panel: Blue lines show recorded oil pressures in in the cylinders A and B during the full-scale tests. Yellow lines show simulated oil pressures in the same cylinders.

Numerical simulations were performed to analyze the influence of a sudden change of the contact area S_{Ice} between the ice and indentation plate. Temporal change of the contact area is modeled by the dependence

$$S_{Ice} = (1 - \alpha\,\mathrm{sech}[0.03\,(t\,100 - 700)])S_{Ice,0}, \tag{24}$$

where the time is calculated in seconds, the coefficient α characterizes the amplitude of the area decrease, and $S_{Ice,0}$ is the initial area of the contact of the indentation plate and ice. The simulations were performed with $\kappa = 1$ and $\alpha = 0.2$, 0.4, and 0.6. The ice force is calculated as $F_{Ice} = S_{Ice}\sigma_c$, where $\sigma_c = 1$ MPa is the ice compression strength and $S_{Ice,0}$=0.1575 m^2. Left panel in Fig. 12 shows that simulated force F_{LC} is similar to the ice force F_{Ice}. Right panel in Fig. 12 demonstrates that displacements of the indentation plate have very insignificant reaction on the changes of the ice load.

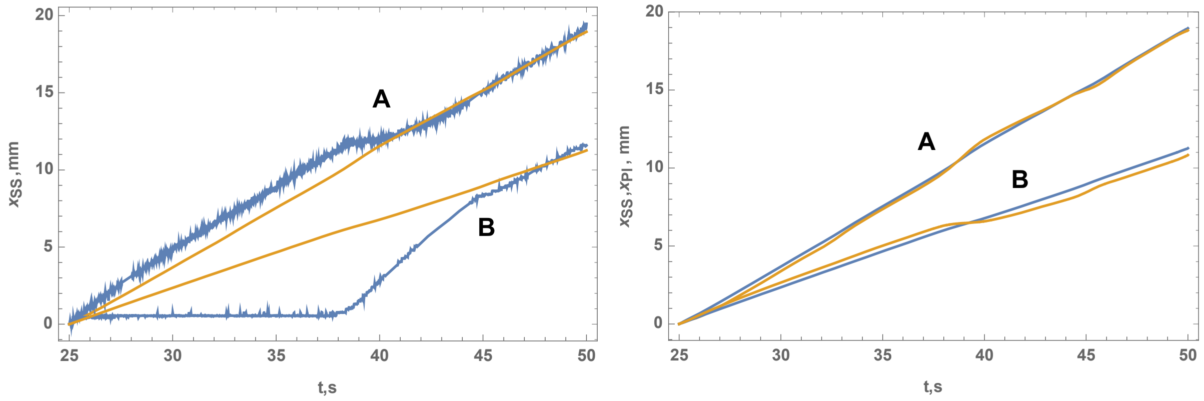

Figure 11. Left panel. Blue lines show records of the stroke sensors in the cylinders A and B during the full-scale tests. Yellow lines show simulated displacements of the plungers. Right panel. Blue lines show simulated displacements x_{SS} and yellow lines show simulated displacements x_{Pl} in the cylinders A and B.

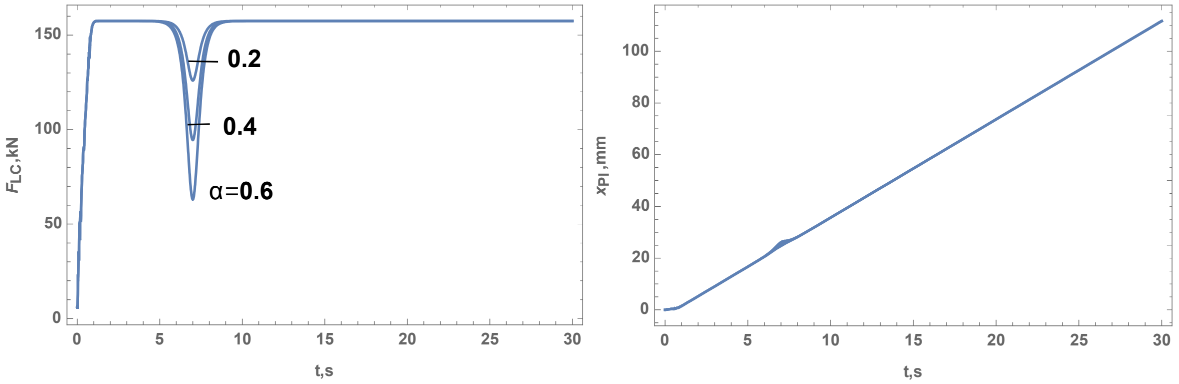

Figure 12. Left panel: Dependencies of the ice load on the indentation plate calculated with local drops of the ice force. Right panel: Displacements of the indentation plate calculated with local drops of the ice force.

CONCLUSIONS

Effective characteristics of the elastic and the viscous properties of the hydraulic rig were estimated from the calibration tests and used in the formulation of a mathematical model of the rig. Numerical simulations were performed to investigate the deviations of displacements and loads measured by the stroke sensors and the load cells mounted in the hydraulic cylinders of the rig from actual displacements of the indentation plate relative to the ice and the ice loads applied to the indentation plate. The oil compressibility was taken into account in the simulations. The loads recorded by the load cells in the full-scale tests on the compression of a short cantilever beam were used as the ice forces applied to the indentation plate. The loads which would be registered by the load cells, and displacements, which would be registered by the stroke sensors were calculated. It is shown that their deviations from the applied ice loads and the deviations of calculated displacements of the indentation plate from those measured during a test are very small. Numerical simulations also showed that displacements of the indentation plate have very small reaction on sudden drops of the ice load applied to the indentation plate when the oil flux into the hydraulic cylinder is constant.

ACKNOWLEDGEMENTS

The authors wish to acknowledge the support of the Research Council of Norway through the Centre for Sustainable Arctic Marine and Coastal Technology (SAMCoT) and AOCEC project of IntPart program. The authors thanks to Dr. Sodhi for useful comments and editing.

REFERENCES

Croasdale, K., R., I974. Crushing strength of Arctic Ice. *Proceedings of a symposium on Beaufort Sea coast and shelf research.* Reed, J.C. and Sater, J.E. (ed), Arlington, Virginia, Arctic Institute of North America, 377-399.

Croasdale, K., R., I977. Indentation tests to investigate ice pressures on vertical piers. *J. Glaciology*, V. 19, 81, 301-312.

Karulin, E., Marchenko, A., Karulina, M., Chistyakov, P., Sakharov, A., Ervik, A., Sodhi, D., 2014. Field Indentation Tests of Vertical Semi-Cylinder on First-Year Ice. *Proc. of the 22th IAHR Symposium on Ice*, Singapore, paper 1125.

Sodhi, D.S., Takeuchi, T., Nakazawa, N., Akagawa, S.,Kato, K., Kamesaki, K., Saka, K., Kurokawa, A., 1998. Medium-scale indentation tests on sea ice at various speeds. *Cold Regions Science and Technology*, 28, 161-182.

Sukhorukov, S., Marchenko, A., 2014. Geometrical stick–slip between ice and steel. *Cold Regions Science and Technology*, 100, 8-19.